LUND UNIVERSITY

Characterization of pulsed gas sources for intense laser field-atom interaction experiments

Altucci, C; Beneduce, C; Bruzzese, R; deLisio, C; Sorrentino, G. S; Starczewski, Tomas; Vigilante, F

[Link to publication]

Characterization of pulsed gas sources for intense laser field–atom interaction experiments

C Altucci†, C Beneduce†, R Bruzzese†, C de Lisio†, G S Sorrentino†, T Starczewski‡ and F Vigilante†

† Istituto Nazionale di Fisica della Materia (INFM) and Dipartimento di Scienze Fisiche, Università di Napoli 'Federico II', Mostra d'Oltremare Pad. 20-80125 Napoli, Italy
‡ Department of Physics, Lund Institute of Technology, PO Box 118, S-22100 Lund, Sweden

Abstract. We describe the application of a tunable differential interferometer to the characterization of pulsed gas valves, operating in the low-pressure regime ($\lesssim 100$ Torr). The spatial profile of the pressure in the gas jet has been studied for piezoelectric and electromagnetic valves in various experimental conditions, for both Ne and Ar gases. Moreover the time response of the valves has been investigated by using, for the first time to our knowledge, the third harmonic generation process. The number of third harmonic photons has been determined as a function of the delay time between a Nd:YAG pump laser pulse and the opening time of the valve, thus allowing the determination of the jet temporal profile. The time dependence of the local pressure in the jet has been studied for various gas pulse durations.

1. Introduction

In recent years pulsed gas beam sources have been extensively used in harmonic [1, 2] and x-ray [3, 4] generation experiments. The use of pulsed gas jets allows the simultaneous fulfilment of two typical requirements of this kind of experiment [5]. Firstly, relatively high atomic densities can be easily achieved in the laser–gas interaction region. Secondly, modest average gas flows are injected into the vacuum chambers, thus requiring simple vacuum systems.

Gas medium features, such as the local density and the geometric shape of the density distribution, play a relevant role both in harmonic and x-ray generation experiments [5, 6]. Thus, the characterization of the spatial profile of the injected gaseous pulse is of importance. In particular, a good knowledge of the gas jet dependence on parameters such as the gas backing pressure $P_{backing}$ and the distance between the nozzle orifice and the laser focus is often required.

The use of pulsed gas sources introduces the problem of synchronizing the gas jet and the laser pulse. Thus, detailed characterization of the temporal profile of the gas jet is also necessary in order to make the laser pulse cross the medium when the local density is at its maximum.

A number of different techniques have been used to characterize the spatial profile of pulsed gas jets. Amongst them we quote, e.g., the induced fluorescence technique

[5] and a technique based on a Mach–Zender interferometer [8]. We present here the application of a tunable differential interferometer [9] to the characterization of pulsed gas jets ($\Delta\tau \approx 1$ ms) operating in a regime of relatively low local pressures ($P_{local} = 10$–100 Torr). This technique, already applied to continous flow studies [9], has several advantages with respect to other methods. Firstly, it is more stable than other interferometric methods because the paths of the two interfering beams are not physically separated. Moreover, as described in the next section, it has a tunable sensitivity which allows the maximization of the signal-to-noise (SNR) ratio by choosing the most appropriate dynamical range. These features turn out to be of fundamental importance in the low-pressure regime.

We have also analysed the temporal profile of the gas jet by means of a new technique: the third harmonic signal, produced by focusing a Nd:YAG laser pulse into the jet, has been measured as a function of the time delay between the rising edge of the electrical signal driving the valve and the laser shot. Since the harmonic yield scales with the square of the local pressure [6], this technique shows a sensitivity higher than that of previous methods [10].

This paper is organized as follows. In sections 2 and 3 we discuss, respectively, the interferometric technique and its application to two different types of valves, namely electromagnetic and piezoelectric. In particular, both the valves were actually used in harmonic generation
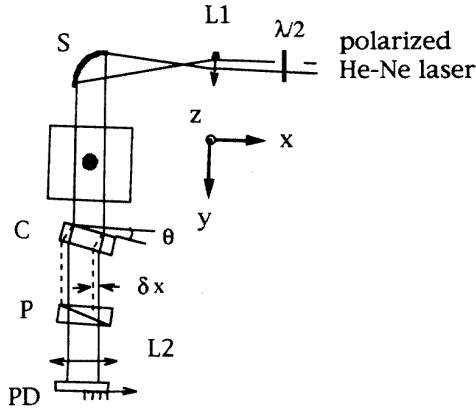
Figure 1. Schematic view of the differential interferometer set-up realized to characterize the gas jet spatially.

experiments [5, 6], thus providing on-line diagnostics of the gaseous medium. In section 4, we describe the gas jet temporal profile characterization. Finally section 5 presents some conclusions.

2. The differential interferometric technique

The scheme of the tunable differential interferometer is presented in figure 1. A sheet of He–Ne light polarized at 45° to the vertical, passes through a calcite crystal C 20 mm long in the light propagation direction y. The horizontally and vertically polarized components are thus displaced by a given amount δx. Thus, the crystal superimposes perpendicularly polarized rays which have travelled parallel paths through the gas target separated by exactly the same distance δx. A polarizer P, positioned after the crystal, selects the common polarization component at 45° to the vertical, of the two orthogonally polarized waves. The resulting interference pattern is a function of the gradient of the path-integrated refractive index. The sheet of He–Ne collimated light is realized by a confocal system consisting of a cylindrical lens L_1 ($f_{L_1} = 6.35$ mm) and a spherical mirror S ($f_S = 250$ mm). The x-dimension of the propagating light sheet is about 40 mm. The detector PD is a fast photodiode with a response time of ~ 4 ns. It is mounted on a precision translation stage in order to scan the interference pattern. The cylindrical lens L_2 ($f_{L_2} = 60$ mm) vertically focuses the beam onto the active cell of the photodiode in order to intensify the signal and to increase the detector dynamic range. It is worth stressing that the refractive effect of the gas medium [11] on the He–Ne beam, as well as wavefront distortion due to gas target turbulence, are negligible in our case. In Xe, for instance, the atomic polarizability is 4×10^{-24} cm^3 so that, for a 2 mm diameter cross section of the jet and a local pressure of $\simeq 100$ Torr, a ray crossing the jet with an incidence angle of $\simeq 45°$ is displaced by $\delta x_{refrac} \approx 2 \times 10^{-3}$ mm. This displacement is negligible with respect to the typical spatial separation, $\delta x \approx 0.1$ mm, of interfering rays which are superimposed by the crystal. The final intensity distribution
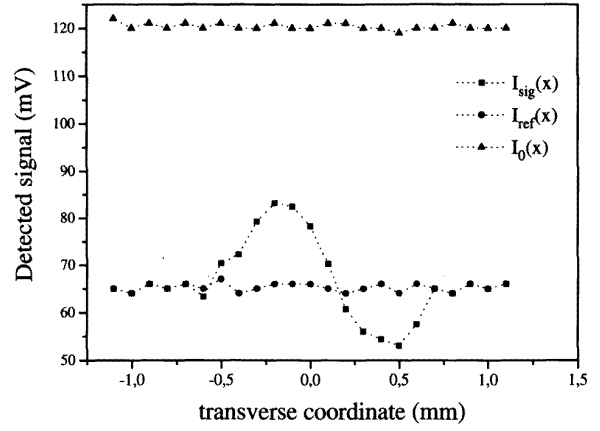

Figure 2. Detected signals: $I_{sig}(x)$ (■) is the intensity distribution of the signal with gas jet, $I_{ref}(x)$ (●) same as $I_{sig}(x)$ but without gas jet, and $I_0(x) = I_{ref}(x) + I_{90}(x)$ (▲) is the total incident intensity distribution where $I_{90}(x)$ is the distribution relative to the perpendicular polarization component without gas jet.

$I(x)$ after the polarizer P is given by [9]

$$I(x) = I_0(x) \sin^2 \left\{ \frac{1}{2} [\delta\phi_\theta + \delta\phi_{err}(x) + \delta\phi_{sig}(x)] \right\} \quad (1)$$

where $I_0(x)$ is the incident intensity, and $\delta\phi_\theta$, $\delta\phi_{err}(x)$, $\delta\phi_{sig}(x)$ are the phase differences between the interfering beams due to the crystal tilting angle θ, the phase error due to the crystal's wavefront distortion, and the differential phase signal from the gas jet respectively. The procedure for measuring the gas jet dependent differential phase $\delta\phi_{sig}$ is the following. At a fixed distance z between the nozzle orifice and the laser focus one measures:

(i) the intensity $I_{sig}(x)$ in the presence of the gas jet;
(ii) the intensity $I_{ref}(x)$ in the same condition as $I_{sig}(x)$, but with no gas jet;
(iii) the intensity $I_{90}(x)$ with no gas jet and with the output polarizer axis rotated 90° in order to measure the incident intensity distribuition $I_0(x) = I_{ref}(x) + I_{90}(x)$.

Once $I_{sig}(x)$, $I_{ref}(x)$, and $I_{90}(x)$ have been measured, the differential phase $\delta\phi_{sig}$, is given by

$$\delta\phi_{sig}(x) = 2\sin^{-1}\left(\sqrt{\frac{I_{sig}(x)}{I_0(x)}}\right) - 2\sin^{-1}\left(\sqrt{\frac{I_{ref}(x)}{I_0(x)}}\right). \quad (2)$$

Thus, by using this method the phase errors due to crystal wavefront distortion are automatically removed in the measurement procedure. By assuming the perfect gas approximation and cylindrical symmetry, the integrated phase $\phi_{sig}(x)$ is related to the pressure field $P(x, y)$ by the Abel integral relation [12]

$$\phi_{sig}(x) = \frac{2\pi}{\lambda_{He-Ne}} \frac{n_0}{P_0} \int_{-\infty}^{\infty} P(x, y) \, dy \quad (3)$$

where P_0 and n_0 are the atmospheric pressure and the refractive index at atmospheric pressure respectively. We have assumed cylindrical symmetry for the gas jet due
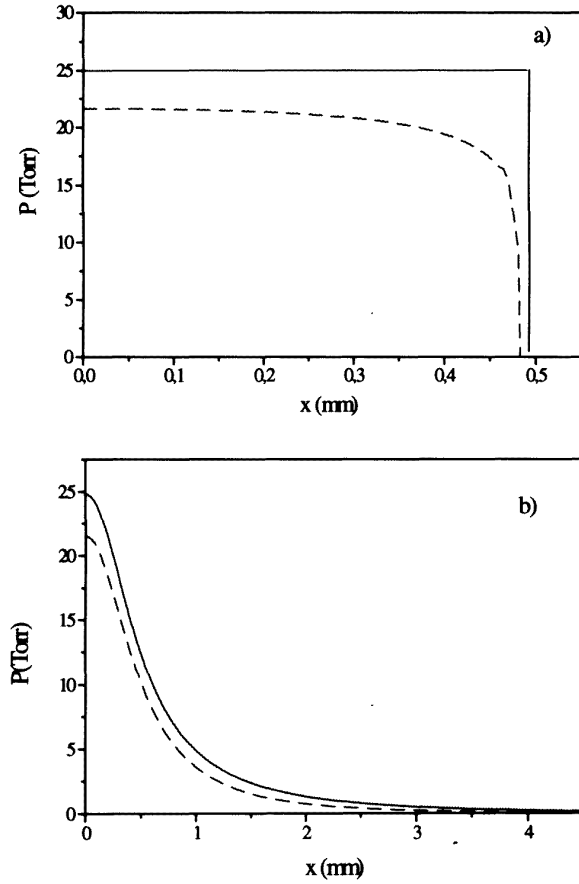
Figure 3. (a) Comparison between a Lorentzian pressure distribution (full curve) and the numerically reconstructed distribution (broken curve) for $\delta x = 0.2$ mm; (b) same as (a) for a top hat distribution (full curve) and the correspondent numerical reconstruction (broken curve). In the simulations the peak pressure into the jet is 25 Torr and the FWHM is 1.0 mm.

to the form of the valve orifice. Thus, by applying the Abel inversion formula [11, 12] to equation (3), the pressure field $P(r)$ reads:

$$P(r) = -\frac{\lambda_{He-Ne}}{2} \frac{P_0}{n_0} \int_r^\infty \frac{\mathrm{d}\phi_{sig}(x)}{\mathrm{d}x} (x^2 - r^2)^{-\frac{1}{2}} \mathrm{d}x \quad (4)$$

where $r = \sqrt{x^2 + y^2}$. In figure 2 typical behaviours of $I_{sig}(x)$, $I_{ref}(x)$ and $I_0(x)$ are shown for the case of Ar.

It is worth noting that since the pressure derivation is independent of the z value, we can reconstruct the full pressure field $P(r, z)$ by repeating the measurement at different values of z.

We have also perfomed resolved gas jet diagnostics. The typical aperture time of the valve has been set around 1.2 ms. The three detected intensities, $I_{sig}(x)$, $I_{ref}(x)$, $I_{90}(x)$ have been measured at each point x, acquiring the maximum amplitude of the detected waveform. While I_{ref} and I_{90} are obviously constant in time, I_{sig} changes, following the gas jet temporal profile. In different conditions of the experiment we have observed that the temporal behaviour of the pressure pulse does not depend on the coordinate r and, in particular, the maximum
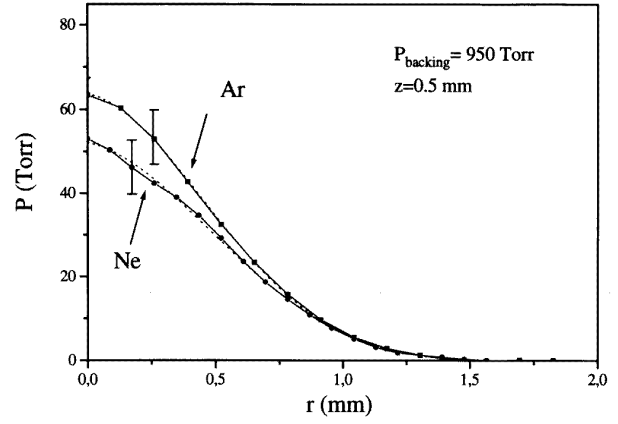

Figure 4. Pressure distribution in Ar and in Ne (——) for $z = 0.5$ mm and $P_{backing} = 950$ Torr with superimposed Gaussian fits ($\cdots\cdots$). Relative errors of experimental points are around 20%, as shown in the case of the points at $r = 0.25$ mm.

amplitude of $I_{sig}(x)$ is always observed at the same time, independently of r. As a consequence, the pressure field in the jet $P(r, t)$ evolves in time in a stationary way, at least for a long time interval centred within the aperture time of the valve. Thus we can separate space and time variables: $P(r, t) = P(r)g(t)$, $g(t)$ being a slowly varying time envelope. Moreover, the time interval spent by the laser in crossing the gas jet is so short ($\simeq 10$ ps) that the pressure field $P(r)g(t)$ can be considered frozen during this time period.

Once ϕ_{sig} is measured, in order to reconstruct the pressure tranverse profile, $P(r)$, we have numerically solved equation (4) by using a code based on the MART algorithm [12, 13]. The code also calculates the uncertainty in the pressure profile. This uncertainty is due to both numerical accuracy and experimental error on the function $\phi_{sig}(x)$.

As the active cell of the detector is a square of side 1.5 mm, it does not define a narrow vertical resolution in the object plane. Thus the vertical resolution of the apparatus is the vertical thickness of the light sheet in the gas jet. The spherical mirror S (figure 1) vertically focuses the light onto the gas jet to a sheet thickness of about 350 μm which represents our vertical spatial resolution.

The horizontal resolution is determined by two factors: how accurately the gradient of path-integrated refractive index, $\delta\phi_{sig}/\delta x$, is estimated and how large is the detector active cell along the horizontal dimension. The first factor is related to the displacement δx of the two orthogonal polarizations and it turns out to be less critical, according to our numerical tests. By assuming a given pressure distribution into the gas jet, we have analytically calculated the path-integrated refractive index, $1/[\delta x \int_{-\infty}^{\infty} \delta\phi_{sig}(r) \mathrm{d}y]$. Then, by considering different incremental ratios corresponding to different displacements δx, we have numerically reconstructed the initial pressure profile using the MART algorithm. Two pressure profiles have been investigated: the Lorentzian profile and the 'top hat' profile. In figure 3 we show the comparison between the initial 'true' distribution and the reconstructed
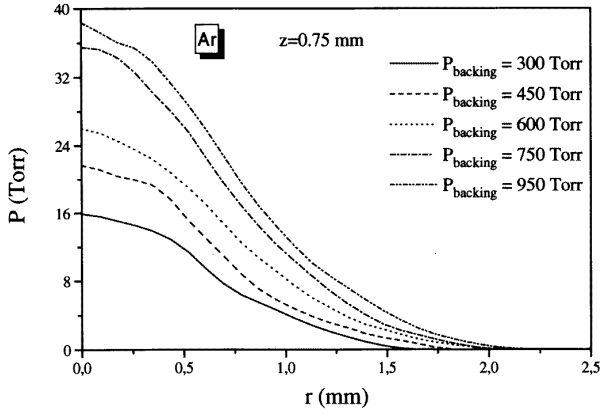
Figure 5. Pressure profiles in Ar for $z = 0.75$ mm and $300 \leq P_{backing} \leq 950$ Torr.

one for a displacement $\delta x = 0.2$ mm, for both Lorentzian and top hat profiles. In the case of the top hat profile there is a rather evident discrepancy between the two curves in proximity of the discontinuity at $x = 0.5$ mm due to numerical uncertainty in the code. In any case, the test has shown that, changing δx by a factor of ten between 50 and 500 μm, the difference between the reconstructed and initial profiles never exceeds 10%.

The second factor affecting the horizontal resolution is the width of the diode active area: in our case, in order to have a better resolution, we have placed a 100 μm wide slit just in front of the photodiode active area. Therefore, our horizontal resolution is ~ 100 μm.

Unlike other interferometric methods, the sensitivity of the tunable differential interferometer can be continuously tuned by tilting the birefringent crystal so that one can choose the most appropriate interferometer response. Due to this tunability, a sensitivity as high as 1/50 of a fringe, corresponding to a local pressure of about 1 Torr, is achieved. It is worth noting that such a sensitivity does not correspond to the reconstructed pressure profile uncertainty, which is also affected by the computational error intrinsic in the inversion procedure of equation (3).

3. Spatial characterization of gas jets

We have used the previously described interferometric technique to characterize the pulsed gas jets produced by two different gas valves, namely, a solenoidal and a piezoelectric valve. This characterization is discussed for both the cases in the following subsections.

3.1. Solenoidal valve jet

We have first characterized the behaviour of the gas jet injected into the interaction chamber by a solenoidal valve designed and realized at CEA laboratories in Saclay (France) [5]. In this valve a driver provides a relatively high-voltage pulse (50–100 V) to a coil which generates a magnetic field: an iron cylinder, coaxial with the coil, is moved up by the magnetic field, carrying the valve poppet against the surface force due to the high-pressure backing
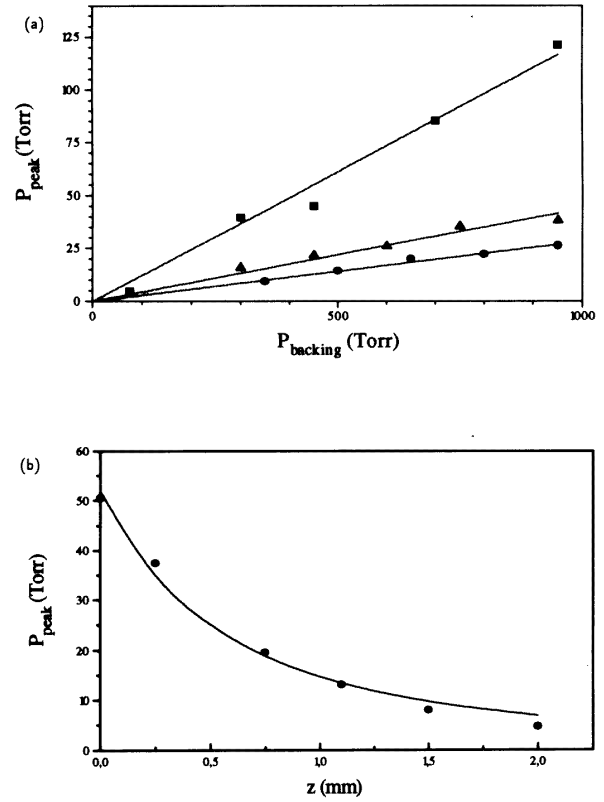

Figure 6. (a) P_{peak} against $P_{backing}$ for three different values of z expressed in mm: $z = 0$ (■), $z = 0.25$ (▲) and $z = 0.75$ (●). The straight lines represent best fits of equation (9). (b) P_{peak} against z for $P_{backing} = 950$ Torr in Ar. The plotted curve represents the behaviour of equation (9) for the same $P_{backing}$ value.

gas (≥ 1 bar), present on the other side of the valve. At the end of the voltage pulse, coil and poppet are pushed down by the pressure force, thus closing the valve orifice. The voltage pulse duration, which sets the valve opening time, ranges within 0.1–10 ms, while the repetition rate is 1–20 Hz. In particular, the following results were obtained with a repetition rate of 10 Hz, an opening time of 1.2 ms, and a pulse voltage of 100 V.

In order to obtain a more collimated and regular gas jet, an Al cylindrical collimator is attached to the orifice of the valve. The collimator is 6 mm long and has an internal diameter of 0.8 mm. The backing pressure $P_{backing}$ measured by a capacitance pressure gauge immediately before the body of the valve ranges within 10–1000 Torr.

We have investigated the jet features for two different gases, Ar and Ne, in the range 50 Torr $\leq P_{backing} \leq$ 1000 Torr. Furthermore, we have characterized the jet for a laser focus–collimator orifice distance z ranging within 0–2 mm. It was not possible to perform jet diagnostics for greater z values because of a too low signal-to-noise ratio. The experimental points in the following data represent an average of 1000 gas pulses.

The jet pressure profiles show a rather regular shape in good agreement with a Gaussian distribution. In figure 4 the pressure profiles for both Ar and Ne are plotted for $z = 0.5$ mm and $P_{backing} = 950$ Torr. The two profiles

are consistent within the error bars even though for Ne the signal-to-noise ratio is lower due to a smaller refractive index of the medium (the Ne polarizability is 5 times smaller than that of Ar).

In figure 5 the pressure profiles in Ar are plotted for $z = 0.75$ mm and different values of $P_{backing}$ (in the range 300–950 Torr).

Some of the most important gas jet features, such as peak pressure, P_{peak}, and jet diameter, D, depend on $P_{backing}$ and z. In particular, we define D as the full width half maximum (FWHM) of the transverse pressure profile.

In figure 6 the peak pressure, P_{peak}, is shown as a function of $P_{backing}$ for three different values of z (a), and versus z for $P_{backing} = 950$ Torr (b).

In figure 7 we show the gas jet diameter, D, versus z, for $P_{backing} = 950$ Torr. The slope of the linear fit represents the total aperture angle, α, of the gas jet. In the above condition, $\alpha \cong 32°$. In general, α does not vary critically with $P_{backing}$, as expected, ranging between 30° and 35° within the investigated interval of backing pressures ($100 \leq P_{backing} \leq 1000$ Torr). The pressure distribution relative uncertainty, estimated by propagating the experimental error through the code, turns out to be around 20%. This error takes into account both the experimental error of the $\delta\Phi_{sig}/\delta x$ curve and the computational error of the algorithm. From the measurements of figure 7 we can infer that the function $D(z, P_{backing})$ describing the dependence of the jet diameter on z and $P_{backing}$ is of the form:

$$D(z, P_{backing}) = 2d_0 + d_1 z + d_2 z P_{backing} \qquad (5)$$

where the coefficients d_0, d_1 and d_3 are given by:

$$d_0 = 0.444 \text{ mm} \qquad d_1 = 0.542 \text{ mm}$$

$$d_2 = 0.000\,198 \text{ Torr}^{-1}.$$

The coefficient d_0 in equation (5) represents the collimator nozzle radius; its nominal value is 0.4 mm. All the measurements of the jet diameter for $z = 0$ and different backing pressures show that $D(0, P_{backing}) = $ constant. By fitting the experimental points with equation (5) for $z = 0$ we obtain $2d_0 = 0.87$ mm. Such good agreement between the nominal and the measured value represents a test of the experimental method.

Moreover, the small coefficient d_2 takes into account the weak dependence of D on $P_{backing}$. By assuming the perfect gas approximation, the gas flow conservation is expressed by:

$$\int_0^\infty r P(r, z)\, \mathrm{d}r = k \qquad (6)$$

where k depends only on the temperature. If we assume for the pressure field the form $P(r, z) = P_{peak}(z) f(r^2/D^2(z))$ with the function f maximum and equal to 1 if $r = 0$, equation (6) reads:

$$P_{peak}(z) = \frac{1}{D^2(z)} k \left(\int_0^\infty \rho f(\rho^2)\, \mathrm{d}\rho \right)^{-1}. \qquad (7)$$

where $\rho = r/D(z)$. The coefficient d_2 is so small that the third term in equation (5) can be neglected without
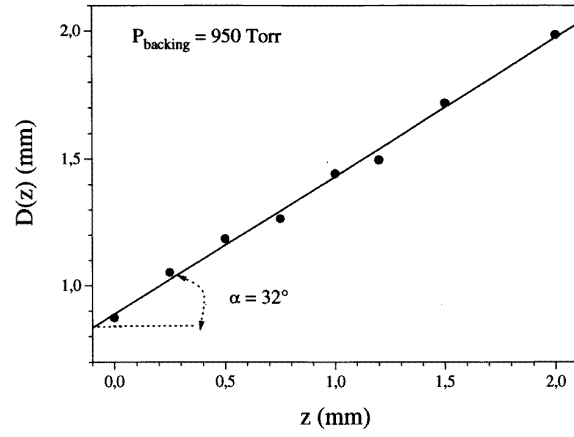
Figure 7. Jet diameter $L(z, P_{backing})$ against z for $P_{backing} = 950$ Torr in Ar. The total aperture of the jet, α, is equal to 32°.

making a relevant error until $z P_{backing} < 1000$ mm Torr. In such a case, $D(z)$ increases linearly with z independently of $P_{backing}$, so that

$$D(z) = 2d_0 + d_1 z \qquad (8)$$

and the jet can be represented as a cone of semi-aperture $\tan^{-1}(d_1)$. Putting equation (8) into equation (7), we obtain for P_{peak}:

$$P_{peak}(z, P_{backing}) = \frac{c_0 P_{backing}}{(z_0 + c_1 z)^2} \qquad (9)$$

where the constants c_0 and c_1, obtained by fitting the experimental points with equation (9), are given by:

$$c_0 = 0.0238 \text{ mm}^2 \qquad c_1 = 0.395.$$

The straight lines of figure 6(a), are the result of a linear fit to the experimental data with equation (5). The agreement with the experimental behaviour is very good. Similarly, the z dependence contained in equation (9) is in optimum agreement with the measurements, as shown in figure 6(b).

The following conclusions can be drawn from our analysis:

- the gas jet behaviour is gas independent;
- the peak pressure, P_{peak}, increases linearly with the backing pressure;
- P_{peak} decays with z in good agreement with a law of the form $(z_0 + \text{constant} \times z)^{-2}$ derived from the gas flow conservation;
- the jet diameter $D(z, P_{backing})$ increases linearly with z and is only slightly dependent on $P_{backing}$.

3.2. Piezoelectric valve jet

The piezoelectric valve [10] differs from the electromagnetic one mainly because it utilizes a piezoelectric crystal to open and close the valve.

The piezoelectric crystal is driven by a voltage pulse, usually of the order of 100–300 V. In this case, the poppet
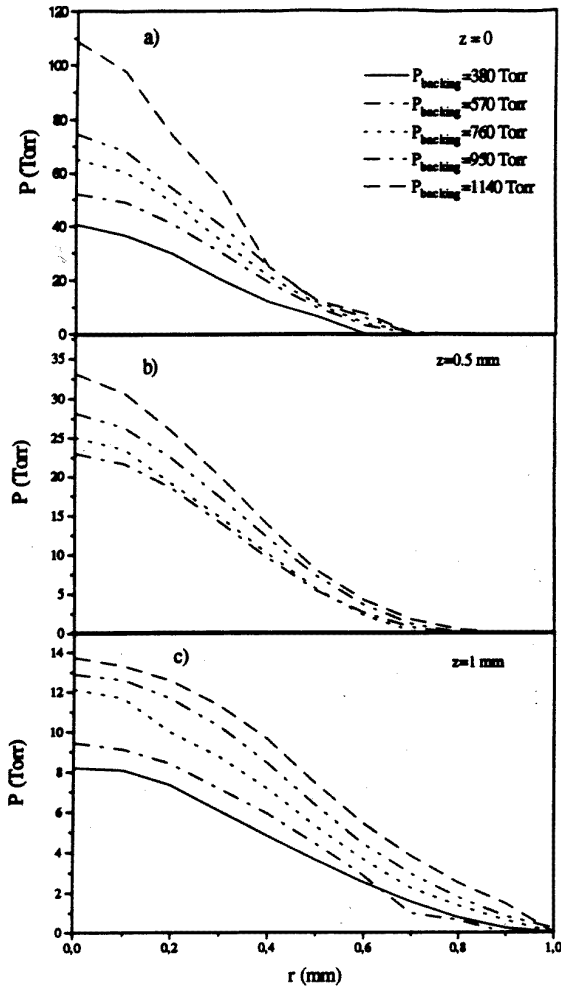
Figure 8. Pressure distribution against radial coordinate for three different values of z: $z = 0$ (a), $z = 0.5$ mm (b) and $z = 1$ mm (c). For each z the profiles are measured for five different values of $P_{backing}$: 380 Torr (——), 570 Torr (— · —), 760 Torr (······), 950 Torr (— ·· —), 1140 Torr (– – –). It can be noticed that the shape of the pressure profile is rather smooth and unchanged under different experimental conditions.
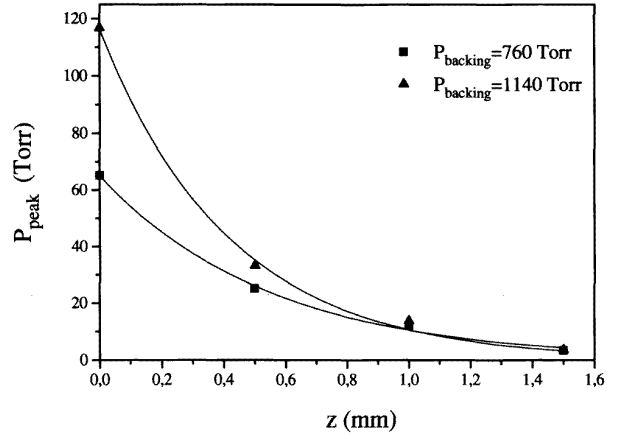

Figure 9. Exponential decay of the peak pressure P_{peak} into the jet against z-coordinate for two different backing pressures: $P_{backing} = 760$ Torr (■) and $P_{backing} = 1140$ Torr (▲).
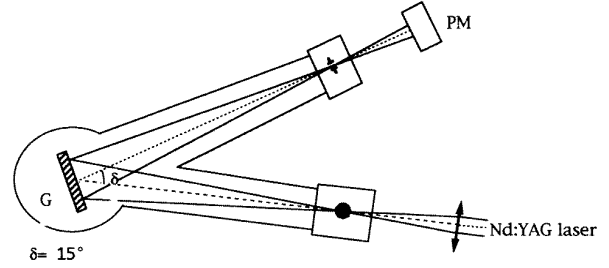

Figure 10. Schematic set-up for the harmonic generation and detection: a Nd:YAG laser pulse is focused by the lens L onto the gas jet. The harmonic signal is detected by means of a monochromator and a photomultiplier.

is fixed to the crystal: when the voltage is applied, the crystal bends up, letting the gas flow into the interaction chamber; with the voltage off, the crystal comes back to its rest position and the poppet closes the valve.

This kind of valve can produce a gas pulse of duration ranging between 100 μs and several milliseconds. It can be operated at a very high repetition rate (typically $\simeq 750$ Hz), namely at repetition rates considerably higher than those of electromagnetic valves. In particular, we have characterized a commercial Lasertechnics valve (model LPV), realized to produce continuous or pulsed atomic and molecular beams. The piezoelectric crystal is driven by 100 V pulses and the backing pressure can range within 0–10 atm. We have operated the valve at a low repetition rate (5 Hz) in order to match the repetition rate of a Nd:YAG laser simultaneously used to generate harmonics into the gas jet [7] and with 300 Torr $\leq P_{backing} \leq 1200$ Torr. A 5 mm long collimator is connected to the nozzle orifice whose

diameter is 0.8 mm. The generated gas pressure profiles are shown in figures 8 and 9. In figure 8 the pressure distribution is plotted against the transverse r coordinate for different values of $P_{backing}$ and for three values of z. Going from $z = 0$ (just below the valve orifice, figure 8(a)) to $z = 1$ mm (figure 8(c)) one can notice that, for each value of $P_{backing}$, the profiles are rather smooth and the peak pressure P_{peak} goes down, while the diameter of the jet, i.e. the FWHM of the profile, increases. The peak pressure behaviour is approximately linear with the backing pressure within the investigated range of $P_{backing}$.

We have plotted the decay of P_{peak} with z for two different backing pressures, as shown in figure 9. The experimental points, averages of 200 gas shots, are well fitted by a decreasing exponential:

$$P_{peak}(z) = P_{peak}^0 \, e^{-z/\lambda} \qquad (10)$$

where P_{peak}^0 is $P_{peak}(z = 0)$, i.e. the pressure just below the output orifice, and λ represents the decay length of the gas jet. We obtained $\lambda = 0.5 \pm 0.1$ mm and $\lambda = 0.4 \pm 0.1$ mm for $P_{backing} = 760$ Torr and $P_{backing} = 1140$ Torr respectively. Such a result suggests that λ is not crucially dependent on $P_{backing}$.

Finally, we have measured the total divergence angle α of the jet which turns out to be about $28°$ for $z = 1$ mm.
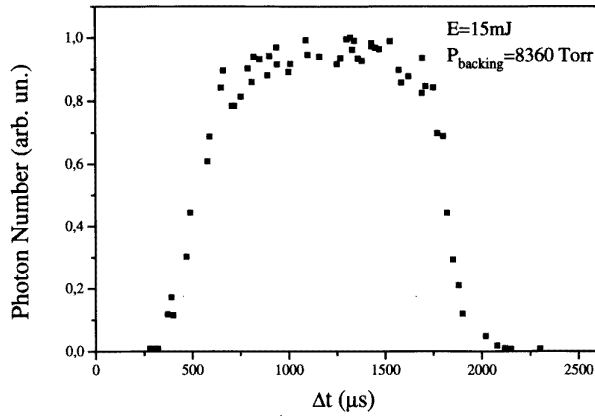
Figure 11. Third harmonic signal against the delay time Δt for an aperture time of 1.2 ms. In this case the electromagnetic valve has been used.

4. Gas jet time profile

In order to characterize the temporal profile of the gas jet we have employed a new technique. With reference to figure 10 a Nd:YAG laser pulse ($\lambda = 1064$ nm, $\tau = 30$ ps, $E_{pulse} \simeq 15$ mJ) is focused by the lens L ($f = 25$ cm) onto the gas jet injected into the interaction chamber through the valve system. The third harmonic radiation generated is detected by means of a monochromator whose output slit is connected to a photomultiplier. We have used a fixed deflection angle configuration ($15°$) and a normal incidence, spherical, holographic grating (Jobin–Yvon), with 1080 grooves mm^{-1} and a radius of curvature 1 m. At the third harmonic wavelength ($\lambda = 354$ nm) the grating and photomultiplier quantum efficiencies are 22% and 25% respectively (see [7] for a full description of the experiment).

We have realized an acquisition system that temporally drives both the laser source and the valve driver unit. We can thus set the time delay Δt between the laser pulse arrival into the chamber and the opening time of the nozzle orifice, and store the detected harmonic signal shot by shot.

In such a way we have studied the third harmonic signal as a function of the delay time Δt. The third harmonic signal, due to the coherence of the generation process, is proportional to the square of the pressure experienced by the laser pulse [14, 5], $P^2(t)$. Thus, the detected number of harmonic photons, through this P^2 dependence, can be used to monitor the time profile of the jet, $P(t)$, in a more sensitive way with respect to other methods. Moreover, since the laser duration (~ 30 ps) is negligible on the timescale of the gas jet evolution, we can monitor the gas pressure instantaneously. Analogously, the laser pulse transit time through the gaseous medium is negligible ($\lesssim 10$ ps).

We have characterized the temporal profile of two pulsed gas jets, the first one produced by a commercial electromagnetic valve (General Valve SERIES 9) operating at 120 Hz repetition rate, and 1 atm $\leq P_{backing} \leq 85$ atm, and the second one produced by the piezoelectric valve (Lasertechnics) described in the previous section.

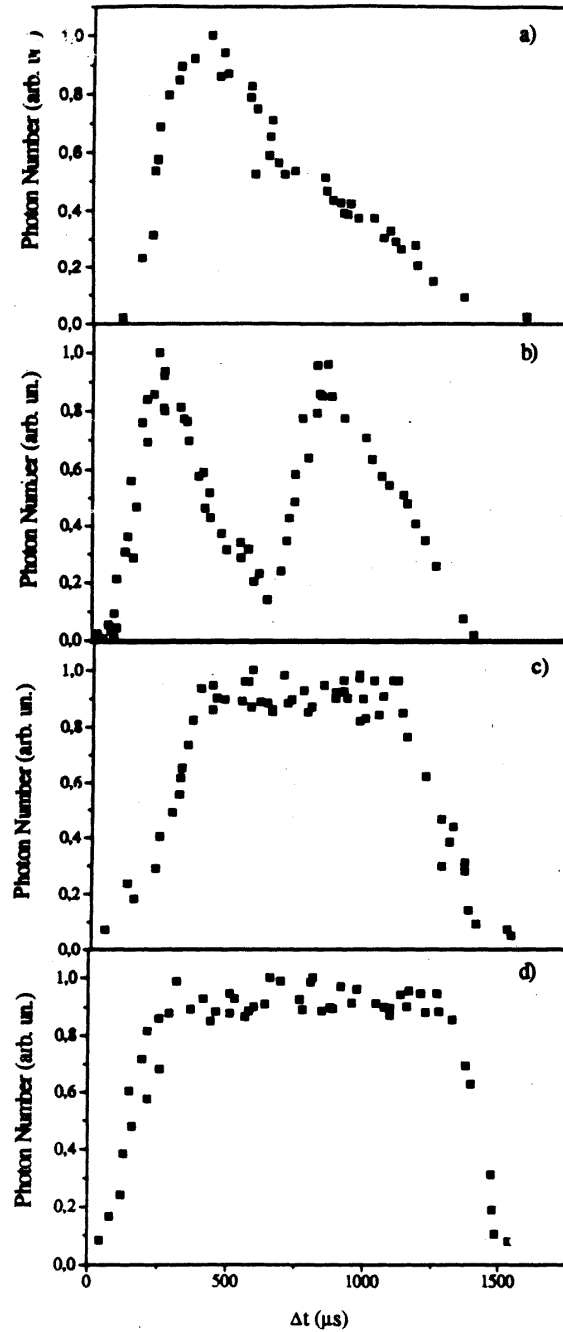**Figure 12.** Third harmonic signal against the delay time Δt for an aperture time of 1.2 ms, by using the piezoelectric valve without the collimator (a) and (b) corresponding to valve aperture times of 0.6 ms and 1.2 ms respectively; and with a collimator (c) and (d), corresponding to aperture times of 0.6 ms and 1.2 ms respectively.

In figure 11 we report the third harmonic signal against delay time Δt for an aperture time of 1.2 ms in the case of the electromagnetic valve. It is possible to notice that the curve is quite regular, with its FWHM corresponding to the valve aperture time. In figure 12 the temporal behaviour of the piezoelectric valve jet is shown. The temporal profile has been analysed in two different configurations of the output nozzle. In the first case, we have used the

standard configuration of the valve, whose nozzle orifice has a nominal diameter of 0.8 mm. We have observed two different types of gas jet time profiles corresponding to distinct values of the aperture times, $\Delta\tau$. Figure 12(a) ($\Delta\tau = 0.6$ ms) shows a regular shape, whereas a double peak structure appears when the aperture time increases to $\Delta\tau = 1.2$ ms) (figure 12(b)). Such behaviour agrees with the temporal response of other similar valves [10] and is probably due to mechanical oscillations of the poppet. In fact, in the case of long $\Delta\tau$ the high backing pressure could make the crystal partially come back and obstruct the orifice, causing an irregular injection of the gas jet and a gas density depletion in the laser focal region. This strongly lowers the harmonic generation efficiency in the central part of the valve aperture time. By attaching a collimator to the nozzle extremity the depletion of the central part of the gas jet is much reduced and we have observed a more regular shape of the gas jet temporal profile in correspondence to all the values of $\Delta\tau$, as reported in figure 12(c) and (d), corresponding to $\Delta\tau = 0.6$ ms and $\Delta\tau = 1.2$ ms respectively.

5. Conclusions

We have discussed the application of a tunable differential interferometer to the characterization of pulsed gas sources. By this method we have been able to determine fully the pressure field $P(x, y, z)$ in the gas jet produced by a commercial and a homemade pulsed gas sources. We have analysed gas pulses about 1 ms long, at relatively low backing pressures (the local peak pressure ranges between 3 and 100 Torr). This technique has a sensitivity as high as $\simeq 1$ Torr and exhibits interesting properties of tunability and flexibility. By employing a more appropriate light detector, such as a fast gated CCD camera with a wide dynamical range, it can also be possible to measure, in real time, the pressure field in the gas jet, shot by shot.

We have also implemented a new technique, based on the coherent process of the third harmonic generation in a gas, that allows one to control, shot by shot, the temporal profile of a gas jet. Since the third harmonic photon yield

scales with the square of the local gas pressure (in the laser–gas interaction region), this technique turns out to be particulary sensitive.

Therefore, such a technique can be considered a well established tool to characterize gas jets in harmonic generation experiments. In particular, it lends itself very well to the optimization of the conversion efficiency [16] and of the optical quality of the harmonic radiation produced, and in the domain of the stimulated emission in the x-ray region.

References

[1] Lago A, Hilbert B and Wallenstein R 1987 *Phys. Rev.* A **36** 3287
[2] Balcou Ph and L'Huillier A 1993 *Phys. Rev.* A **47** 1447
[3] Amendt P, Eder D C and Wikes S C 1991 *Phys. Rev. Lett.* **66** 2589
[4] Borgström S, Fill E, Larsson J, Starczewski T, Steingruber J, Svanberg S and Wahlström C G 1994 X-ray spectra of optical-field ionized plasmas *ECLIM (Oxford) Septemper 19–23 1994*
[5] Lompré L A, Ferray M, L'Huillier A, Li X F and Mainfray G 1988 *J. Appl. Phys.* **63** 1791
[6] L'Huillier A, Lompré L A, Mainfray G and Manus C 1992 *Atoms in Intense Laser Fields* ed Gavrila (New York: Academic) p 139
[7] de Lisio C, Beneduce C, Bruzzese R, Solimeno S, Sorrentino G S, Vigilante F and Altucci C 1995 *Phys. Rev.* E **52**
[8] de Lisio C 1992 Processi multifotonici non risonanti in atomi di gas rari *PhD Thesis*
[9] Faris G W and Hertz H M 1989 *Appl. Opt.* **28**
[10] Andresen P, Faubel M, Haeusler D, Kraft G, Luelf H W and Skofronick J G 1985 *Rev. Sci. Instrum.* **56** 2038
[11] Faris G W and Byer R L 1987 *Science* **238** 1700
[12] Bracewell R 1965 *The Fourier Transform and its Applications* (New York: McGraw-Hill) 262
[13] Fleurier C and Chapelle J 1973 *Comp. Phys. Commun.* **7** 200
[14] Hertz H M 1986 *Appl. Opt.* **25** 914
[15] Rosman R, Gibson G, Boyer K, Jara H, Luk T S, McIntyre I A, McPherson A, Solem J C and Rhodes C K 1988 *J. Opt. Soc. Am.* B **5** 1237
[16] Altucci C, Starczewski T, Mevel E, Carré B, L'Huillier A and Wahlström C-G 1995 The influence of atomic density in high harmonic generation *J. Opt. Soc. Am.* B